Available online at www.sciencedirect.com

ScienceDirect

Ceramics International 40 (2014) 4759–4765

CERAMICS INTERNATIONAL

www.elsevier.com/locate/ceramint

Compositional dependence of dielectric and ferroelectric properties in $BiFeO_3$–$BaTiO_3$ solid solutions

Hailong Zhang[a,b,*], Wook Jo[a], Ke Wang[a], Kyle G. Webber[a]

[a]*Institute of Materials Science, Technische Universität Darmstadt, Darmstadt 64287, Germany*

[b]*State Key Laboratory for Advanced Metals and Materials, University of Science and Technology Beijing, Beijing 100083, China*

Received 5 August 2013; received in revised form 5 September 2013; accepted 5 September 2013

Available online 12 September 2013

Abstract

Polycrystalline $(1-x)BiFeO_3$–$xBaTiO_3$ $(0.11 \le x \le 0.5)$ ceramics have been prepared by the solid-state reaction method to investigate their phase structure, dielectric, ferroelectric, and field-induced strain behaviors. The phase was found to change from rhombohedral in $BiFeO_3$-rich compositions to pseudocubic at a $BaTiO_3$ content of $x=0.33$. The room-temperature dielectric permittivity increased with increasing $BaTiO_3$ content regardless of phase structure, except for a small dielectric permittivity peak additionally observed at $x=0.33$. The $(1-x)BiFeO_3$–$xBaTiO_3$ solid solutions displayed a maximum in permittivity at temperatures (T_m) above 300 °C in the compositional range of $0.2 \le x \le 0.5$. The frequency dependence of high-temperature dielectric properties suggests that $BiFeO_3$–$BaTiO_3$ is a relaxor ferroelectric. Normal ferroelectric loops and large electric field-induced strains were observed for the $BiFeO_3$–$BaTiO_3$ ceramics. The $BiFeO_3$–$BaTiO_3$ shows a promising candidate for high temperature ferroelectric applications.

Keywords: A. Powders: solid state reaction; C. Dielectric properties; C. Ferroelectric properties; D. $BaTiO_3$ and titanates

1. Introduction

$BiFeO_3$ has received significant attention as a multiferroic material, simultaneously displaying both ferroelectricity and ferromagnetism in the same phase. The processing of bulk $BiFeO_3$ ceramics often results in the production of impurities such as $Bi_2Fe_4O_9$, $Bi_{25}FeO_{40}$, or $Bi_{46}Fe_2O_{72}$ [1]. It has been demonstrated that by forming solid solutions with other perovskites, the structure of $BiFeO_3$ is stabilized and the formation of second phases can be hindered [2,3]. Among the potentially important systems, $BiFeO_3$–$BaTiO_3$ represents such a solid solution and is attracting interest due to its high temperature strain capabilities and lead-free nature [4].

$BiFeO_3$–$BaTiO_3$ compositions have demonstrated relatively high Curie temperatures (T_c) [5] and thus allow for potential piezoelectric applications at elevated temperatures. Piezoelectric actuators, sensors, and transducers used in medical, aerospace, and automotive industries require high operating temperatures [6]. $Pb(Zr,Ti)O_3$ (PZT), currently the most commercially used piezoelectric material, however, is limited to temperatures below 250–300 °C due to limited depoling temperatures and a tendency to rapidly age [6]. For this reason, $BiFeO_3$–$BaTiO_3$ is an attractive candidate for high-temperature piezoelectric applications.

In spite of the potential technical importance of $BiFeO_3$–$BaTiO_3$ ceramics in piezoelectric applications, their dielectric and ferroelectric properties are still not well understood. While magnetic properties have been extensively measured in $BiFeO_3$–$BaTiO_3$ solid solutions [2,7–12], the dielectric and ferroelectric properties are relatively less investigated, with the sparsely reported results showing significant variations between investigations. Furthermore, misunderstanding with some transition temperatures in $BiFeO_3$–$BaTiO_3$ occurs widely. $BiFeO_3$–$BaTiO_3$ has cations with various valences in both A and B sites of the ABO_3 perovskite cell, which meets a necessary condition for relaxor ferroelectrics [13]. This corresponds well with the broad dielectric maxima that has been observed in $BiFeO_3$–$BaTiO_3$ solid solutions [3,14]. Nevertheless, many researchers [3,5] still confuse T_m, the temperature at which dielectric

*Corresponding author at: State Key Laboratory for Advanced Metals and Materials, University of Science and Technology Beijing, Beijing 100083, China. Tel.: +86 10 6233 2258; fax: +86 10 6233 3447.

E-mail address: hlzhang@ustb.edu.cn (H. Zhang).

0272-8842/$ - see front matter © 2013 Elsevier Ltd and Techna Group S.r.l. All rights reserved.
http://dx.doi.org/10.1016/j.ceramint.2013.09.020

permittivity exhibits a maximum, with the Curie point T_c, a term reserved for normal ferroelectrics. In addition, $BiFeO_3$ as a ferromagnetic material has a Neel temperature (T_N) of 370 °C [15]. Thus, $BiFeO_3$–$BaTiO_3$ also has a characteristic temperature corresponding to magnetic ordering transition. The T_N has been revealed to decrease with increasing $BaTiO_3$ content in $BiFeO_3$–$BaTiO_3$ solid solutions [8,13]. T_N, however, is also confused with T_m in the literature [2].

$BiFeO_3$–$BaTiO_3$ has been claimed to be a ferroelectric material [9,16], although saturated polarization-electric field (*P–E*) loops [9,16], which are prerequisite for ferroelectricity [17], are rarely reported. The absence of proper ferroelectric hysteresis is partly due to excessively large coercive field and partly due to high conductivity, both of which are inherent in $BiFeO_3$ [18,19]. It is well known that Fe^{3+} in $BiFeO_3$ is readily reduced to Fe^{2+}, resulting in the formation of oxygen vacancies to retain the charge neutrality; thus causing thermally activated hoping conduction [2]. This results in $BiFeO_3$–$BaTiO_3$ displaying a high electrical conductivity. Doping with Sc [12], Mn [5], Cr [20], or Dy [21] has been found to decrease the conductivity of $BiFeO_3$–$BaTiO_3$, as evidenced by the formation of saturated *P–E* loops. Mn doping was shown to be highly effective in enhancing the resistivity of $BiFeO_3$–$BaTiO_3$ ceramics [5], resulting in well formed hysteresis loops similar to those observed in $BiFeO_3$ films [22]. In this work, we will show that saturated *P–E* loops can also be attained in $BiFeO_3$–$BaTiO_3$ bulk ceramics even without Mn modification. The key is to use a small sample, which is helpful to decrease the number of defects that are closely connected with high electrical conductivity. As such, a high electric field can be applied and a saturated *P–E* loop is induced in the $BiFeO_3$–$BaTiO_3$ bulk samples.

Electric field-induced strains in $BiFeO_3$–$BaTiO_3$, which are of interest for actuation applications, have been to date rarely reported. The $(1-x)BiFeO_3$–$xBaTiO_3$ solid solutions show rhombohedral symmetry when $x < 0.33$, tetragonal symmetry when $x > 0.94$, and cubic symmetry when $0.33 < x < 0.94$ [3]. Leontsev et al. [5,23] have reported strains for Mn-modified $0.75BiFeO_3$–$0.25BaTiO_3$ and $0.67BiFeO_3$–$0.33BaTiO_3$ ceramics, both with a rhombohedral symmetry. So far the electric field-induced strain has not been reported for cubic-structured $BiFeO_3$–$BaTiO_3$. It is generally thought that cubic structure precludes ferroelectricity, although it has been suggested that rhombohedrally distorted polar nanoregions exist in a cubic-structured $0.6BiFeO_3$–$0.4BaTiO_3$ [24]. The nanoscale domain patterns in poled bulk samples can be induced to form long-range ordered bands of uniform polarization [23,25,26]. In theory, ferroelectric behavior can also be observed in such cubic-structured $BiFeO_3$–$BaTiO_3$ solid solutions. We will show that electric field-induced strain is observed in the cubic-structured $BiFeO_3$–$BaTiO_3$.

In this article, pure phase $(1-x)BiFeO_3$–$xBaTiO_3$ solid solutions are produced by the solid-state reaction method with a wide compositional range of $0.11 \le x \le 0.5$. The dielectric and ferroelectric properties are investigated in relation to $BaTiO_3$ content and compared to previous investigations. The results are helpful to clarify the above-mentioned issues existing in $BiFeO_3$–$BaTiO_3$.

2. Experimental methods

The raw materials used were Bi_2O_3 (99.975% purity, Alfa Aesar), Fe_2O_3 (99.5% purity, Alfa Aesar), $BaCO_3$ (99.8% purity, Alfa Aesar), and TiO_2 (99.6% purity, Alfa Aesar). The investigated compositions were $(1\text{-}x)BiFeO_3$–$xBaTiO_3$ (x=0.11, 0.18, 0.2, 0.25, 0.3, 0.33, 0.4, and 0.5). The powders were stoichiometrically mixed according to the chemical formula and then ball-milled for 24 h at 250 rpm using ZrO_2 balls in a polymer jar with ethanol as a milling media. The powder mixtures were calcined for 5 h at 830–860 °C, depending on the composition. An additional ball-milling step was conducted for 24 h at 250 rpm following calcination to achieve better homogeneity of the final powders. The synthesized powders were die-pressed at 200 MPa, followed by cold isostatic pressing (CIP) at 300 MPa. The CIPed compacts were sintered for 2 h at 870–1030 °C, depending on the composition. During sintering, the compacts were covered with calcined powders with the same compositions to avoid the volatilization of Bi element. Disc-shaped samples with a size of Ø 7 mm × 1 mm were obtained.

X-ray diffraction (XRD, D8 Advance, Bruker, Germany) analysis was performed on the bulk samples to detect the phase structure. The Ø 7 mm × 1 mm samples were pasted with silver-electrodes on both circular surfaces for electrical measurements. Room-temperature dielectric properties were measured by an impedance analyzer (HP4192A, Hewlett-Packard Company, USA). The dielectric properties were also measured from room temperature to 600 °C at a constant heating rate of 2 °C/min, in the frequency range of 10^2–10^6 Hz. The Ø 7 mm × 1 mm samples were ground to a thickness of 0.5 mm to perform macroscopic ferroelectric characterization. The *P–E* hysteresis loops and electric field-induced strains were simultaneously measured in a silicone oil bath equipped with a Sawyer–Tower circuit and a linear variable differential transformer. The measurements were performed at a frequency of 4 Hz.

3. Results and discussion

3.1. Phase structure

Fig. 1(a) shows the XRD patterns of the sintered $BiFeO_3$–$BaTiO_3$ samples. It can be seen that pure perovskite-structured $BiFeO_3$–$BaTiO_3$ bulk samples were produced. Kumar et al. [3] demonstrate that in $(1-x)BiFeO_3$–$xBaTiO_3$ solid solutions, the phase is rhombohedral when $x \le 0.3$ and is cubic when $x \ge 0.4$, leaving a rhombohedral-to-cubic phase boundary at x=0.33. By data fitting, our results show that the phase identification was close to PDF# 71–2494 (rhombohedral symmetry) when $x \le 0.3$ and to PDF# 75–0210 (cubic symmetry) when $x \ge 0.4$, consistent with literature [3]. The lattice parameters were determined to be $a=b=0.5588$ nm and $c=1.3867$ nm for the rhombohedral-structured $BiFeO_3$–$BaTiO_3$, and $a=0.3996$ nm for the cubic-structured $BiFeO_3$–$BaTiO_3$. $BiFeO_3$ is a rhombohedrally distorted cubic perovskite. The distortion is obtained by the cooperative

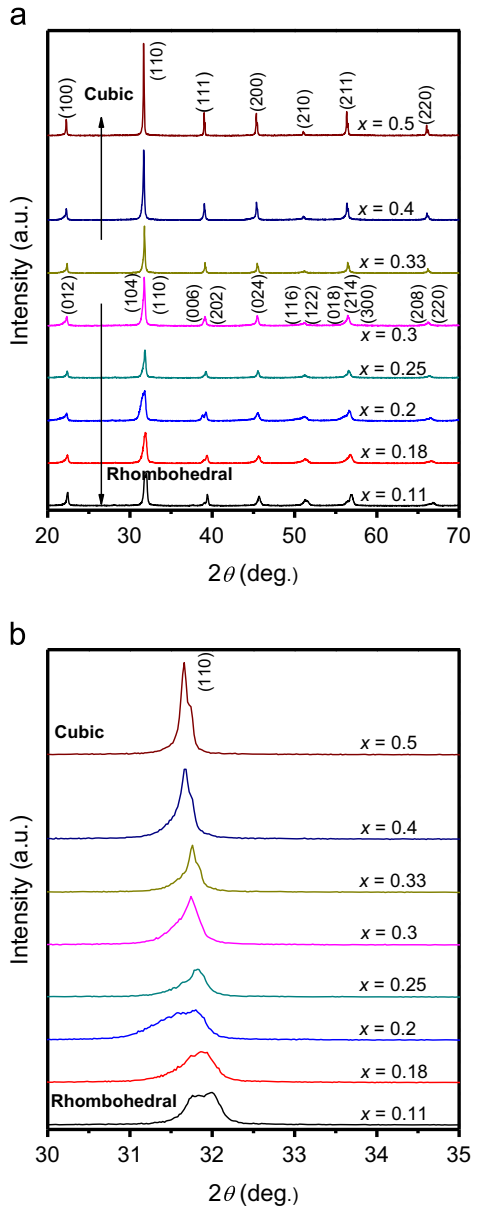

Fig. 1. XRD patterns of (a) the $(1-x)BiFeO_3$–$xBaTiO_3$ solid solutions and (b) enlarged reflection lines.

rotation of an octahedral along the (111) direction. The interaction of 6*p* and 6*s* orbitals of Bi^{3+} plays a critical role in causing the octahedral distortion [27]. Addition of Ba^{2+} with empty *p* orbitals hampers the movement of Bi ion and reduces the structural distortion. At a critical $BaTiO_3$ concentration, the movement completely ceases and a cubic distortion is thus induced in the $BiFeO_3$–$BaTiO_3$ solid solution [3].

As shown in Fig. 1(b), the (110) peak is broadened with increasing *x* from 0.11 to 0.2, and is narrowed with further increasing *x* from 0.25 to 0.5. The peak broadening could be explained by the mixed occupations of Bi and Ba ions in A site and Fe and Ti ions in B site. The random displacements can cause different 2θ reflections, leading to the broadening effect in XRD [16]. With the increase in cubic phase content, the XRD peaks are narrowed. For example, the width of (110) peaks in $x=0.25$ and 0.3 is much narrower than $x=0.2$, since $x=0.3$ is close to the cubic-structured composition of $x=0.33$. The peak splitting of (110) can be observed at $x=0.11$, showing a characteristic of rhombohedral structure, but the peak splitting is covered by peak broadening at higher *x* values. It can be seen from Fig. 1(b) that the diffraction peak shifted towards low angles with increasing $BaTiO_3$ content. The radius of Ti^{4+} (0.068 nm) is similar to that of Fe^{3+} (0.064 nm), but the radius of Ba^{2+} (0.134 nm) is much larger than that of Bi^{3+} (0.096 nm). As a result, $BaTiO_3$ replacing $BiFeO_3$ will lead to an expansion of perovskite crystals.

3.2. Room-temperature dielectric properties

Fig. 2 shows the dielectric properties of the $BiFeO_3$–$BaTiO_3$ solid solutions measured at room temperature. The dielectric permittivity and loss observed for the $BiFeO_3$–$BaTiO_3$ solid solutions are highly consistent with results independently measured by Leontsev et al. [5], whereas the dielectric permittivity is much higher than the values reported elsewhere [12]. Table 1 summarizes the dielectric and ferroelectric properties of $BiFeO_3$–$BaTiO_3$ solid solutions. As shown in Table 1, at the same measuring frequency of 1 kHz, the dielectric permittivity and loss for $x=0.25$ and 0.33 are close to reported values [5].

The cubic-structured $(1\text{-}x)BiFeO_3$–$xBaTiO_3$ ($x=0.4$, 0.5) had higher dielectric permittivity (ε_r) than the rhombohedral-structured solid solutions ($0.11 \le x < 0.33$). This is owing to the larger dielectric permittivity of $BaTiO_3$ than $BiFeO_3$ ($\varepsilon_r \approx 40$ [28]). Interestingly, an anomaly in ε_r value was observed at $x=0.33$, which is the phase boundary between rhombohedral and cubic symmetries. A large body of literature has suggested that peaked permittivity is attained at a phase transition boundary in perovskite solid solutions like $BaTiO_3$-$BaZrO_3$ [29] and $KNbO_3$-$NaNbO_3$ [30]. This kind of dielectric anomaly is ascribed to the so-called morphotropic phase boundary (MPB) effect [31]. However, the peaked ε_r value of 819 found at the phase boundary was much lower than that observed at $x=0.5$ ($\varepsilon_r=1290$). This suggests that the substitution level of $BaTiO_3$ plays a more important role than phase instability in determining the dielectric properties of $BiFeO_3$–$BaTiO_3$.

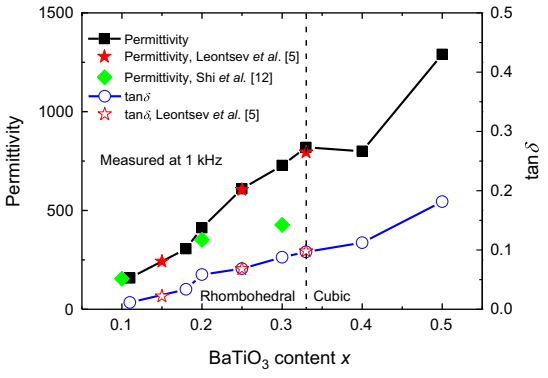

Fig. 2. Compositional dependence of dielectric permittivity and loss of the $(1-x)BiFeO_3$–$xBaTiO_3$ solid solutions at room temperature.

Table 1
Dielectric and ferroelectric properties of the $(1-x)BiFeO_3$–$xBaTiO_3$ solid solutions.

$BaTiO_3$ content x	ε_r [a]	tanδ [a]	T_m [a] (°C)	P_r [b] (μC/cm^2)	E_c [b] (kV/mm)	s_{max} [b] (%)
0.11	158	0.0113				
0.18	306	0.0335				
0.2	412	0.0585	570			
0.25	610	0.0683				
0.25 (Leontsev et al. [5])	605	0.0680				
0.3	728	0.0876		22.4	3.2	0.14
0.33	819	0.0969	592	19.6	2.9	0.15
0.33 (Leontsev et al. [5])	795	0.0980	605	15.2 [c]	2.1 [c]	0.18 [c]
0.4	800	0.1122	545	13.0	2.2	0.12
0.5	1290	0.1816	321			

[a] Measured at $f=1$ kHz.
[b] Measured at $E_{max}=7$ kV/mm.
[c] Mn-modified samples.

The measured tanδ values were below 0.2 for all the compositions investigated, and even below 0.1 for $0.11 \le x \le 0.33$, which are lower than previously reported values [8,12]. It is noted that the dielectric loss increased monotonically with increasing $BaTiO_3$ content regardless of phase structure. As shown in Fig. 2, the dielectric loss increases from 0.0113 to 0.1816 with increasing x value from 0.11 to 0.5. The finding is consistent with literature [5], where the dielectric loss of $(1-x)BiFeO_3$–$xBaTiO_3$ increases from 0.022 to 0.098 with increasing x value from 0.15 to 0.33. The behavior was unexpected; $BaTiO_3$ is generally thought to be more stable and have less electric leakage than $BiFeO_3$. Possible reason for the unexpected behavior is that the addition of $BaTiO_3$ could push a possible phase transition below room temperature to higher temperatures. More detailed discussion is provided later in association with the permittivity–temperature curve of $(1-x)BiFeO_3$–$xBaTiO_3$ solid solutions.

3.3. Temperature-dependent dielectric properties

Fig. 3 shows the temperature-dependent dielectric properties of the (1-x)$BiFeO_3$–$xBaTiO_3$ solid solutions recorded during heating. In the temperature range of 20–600 °C, two peaks were observed in the permittivity–temperature curves. The temperature at maximum permittivity T_m was determined to be 570 °C, 592 °C, and 545 °C for $x=0.2$, 0.33, and 0.4, respectively.

Another anomaly in permittivity below T_m should be characterized as the Neel temperature (T_N), at which the magnetic ordering of $BiFeO_3$–$BaTiO_3$ is altered. $BiFeO_3$ is reported to have a T_N of 370 °C, demonstrated by neutron diffraction [15]. Since $BiFeO_3$–$BaTiO_3$ solid solutions exhibit magnetoelectric coupling effect [2,9], the Neel temperature can be detected from the permittivity–temperature curve. As shown in Fig. 3, the T_N of (1-x)$BiFeO_3$–$xBaTiO_3$ were determined to be 276 °C and 304 °C for $x=0.33$ and 0.4, respectively. The T_N value increased with increasing x from 0.33 to 0.4. It is reported that the T_N of (1-x)$BiFeO_3$–$xBaTiO_3$, however, decreases with increasing x from 0.1 to 0.3 [8]. The larger T_N observed at $x=0.4$ than $x=0.33$ could be related to the

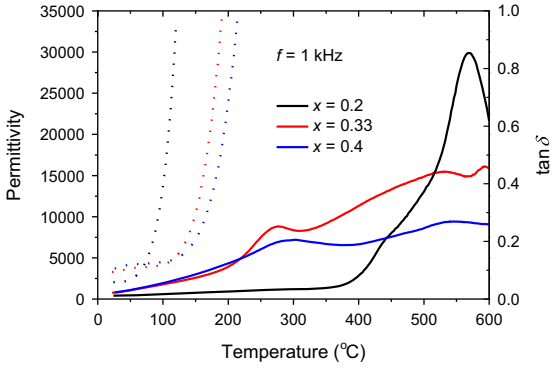

Fig. 3. Temperature dependence of dielectric permittivity and loss of the $(1-x)BiFeO_3$–$xBaTiO_3$ solid solutions.

phase transition of rhombohedral-to-cubic at $x=0.33$. According to the Landau–Devonshire theory [32], this type of dielectric anomaly in magnetoelectrically ordered systems is an effect of intrinsic magnetoelectric coupling. Kim et al. [21] have used high-temperature neutron diffraction and dielectric measurements to determine the T_N for Dy-modified $BiFeO_3$–$BaTiO_3$. Several authors have also reported a similar kind of dielectric anomaly in the vicinity of Neel temperature [11,33].

As shown in Fig. 3, the dielectric loss is too large to be measured above a certain temperature, suggesting highly conductive characteristics of the unmodified $BiFeO_3$–$BaTiO_3$. Above a critical temperature (~75 °C), the loss decreased with increasing x value. Below the temperature, however, the loss increased with increasing x value. This explains why the dielectric loss measured at room temperature increased with increasing $BaTiO_3$ content, as shown in Fig. 2. A reasonable explanation of the critical temperature is that there could be a phase transition in $BiFeO_3$–$BaTiO_3$ below room temperature, which is beyond the temperature range investigated. Since dielectric loss maximum generally occurs near a phase transition temperature, the proximity to phase transition temperature will increase the values of dielectric loss observed. The increase of $BaTiO_3$ content may push the possible phase transition to higher temperatures, which is similar to the role of $BaZrO_3$ content in shifting the phase transition temperature

in $BaTiO_3$-$BaZrO_3$ system [29]. As a result, the dielectric loss observed below 75 °C increases with increasing $BaTiO_3$ content from $x=0.2$ to 0.4. Above the critical temperature, the dielectric loss dramatically rises for all the three compositions, due to the thermally activated space charge polarization.

In order to clearly understand the physical meaning of the permittivity anomaly peaks observed in the permittivity–temperature curves, the characteristic temperatures were collected and compared with literature, as shown in Fig. 4. In previous studies, the characteristic temperatures reported for $BiFeO_3$–$BaTiO_3$ are explained with different physical mechanisms. These characteristic temperatures can be divided into two regions. The first characteristic temperature is T_m at which the highest dielectric permittivity is observed in permittivity–temperature curve. Wang et al. [16] have also employed high-temperature neutron diffraction to determine the T_m of $BiFeO_3$–$BaTiO_3$. The data reported in this region varied widely. For example, the T_m reported for $x=0.2$ varies greatly from 475 °C to 740 °C. Some authors have measured their samples only at low temperatures [3,14,25,34], but they claim that the observed permittivity anomaly is for T_m. Leontsev et al. [5] have detected a depolarization temperature T_d just below T_m in Mn-modified $BiFeO_3$–$BaTiO_3$. Although the reported data may vary among various investigators, it is likely that the reported characteristic temperatures below T_m are actually T_d [35]. The second characteristic temperature below T_m is characterized as T_N. As mentioned above, several groups have observed similar dielectric anomaly in the vicinity of Neel temperature in $BiFeO_3$-based materials [8,11,21,33]. Our results are shown to be in agreement with literature and thus constitute a T_N-x map for $(1-x)BiFeO_3$–$xBaTiO_3$ that covers a wide compositional range from x=0 to 0.5.

Fig. 5 shows the frequency dependence of dielectric permittivity and loss of the $BiFeO_3$–$BaTiO_3$ solid solutions. With increasing frequency, the value of permittivity was reduced and the permittivity peak shifted towards high temperatures, as summarized in Fig. 6. At the same time, the value of tanδ at low temperatures was increased with increasing frequency. These findings suggest relaxor behavior of the $BiFeO_3$–$BaTiO_3$ solid solutions. The temperature range in which dielectric loss is measurable is also markedly enlarged with increasing frequency. This implies that the conduction mechanism is associated with mobile ions or vacancies. When the jumping of charge carriers cannot follow the applied electric fields at high frequencies, the relaxation polarization is suppressed [36]. In the present samples, the mobile charge carriers should be oxygen vacancies that are introduced by the reduction of Fe^{3+} to Fe^{2+}.

Although both $BiFeO_3$ and $BaTiO_3$ are characterized as normal ferroelectrics, $BiFeO_3$–$BaTiO_3$ solid solutions are suggested to be relaxor ferroelectrics. The phase structure of $BiFeO_3$ is changed by the mixture of various valences cations in both A and B sites of the ABO_3 perovskite cell. Bi^{3+} and Ba^{2+} are mixed in the A sites and Fe^{3+} and Ti^{4+} in the B sites of $BiFeO_3$ crystals. These cations have different Pauling's electronegativities and also have different ionic radii. The difference has induced the change in phase structure of $BiFeO_3$.

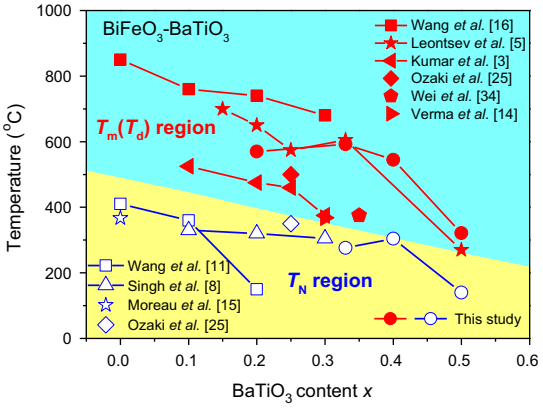

Fig. 4. Compositional dependence of characteristic temperatures for $(1-x)$ $BiFeO_3$–$xBaTiO_3$ solid solutions.

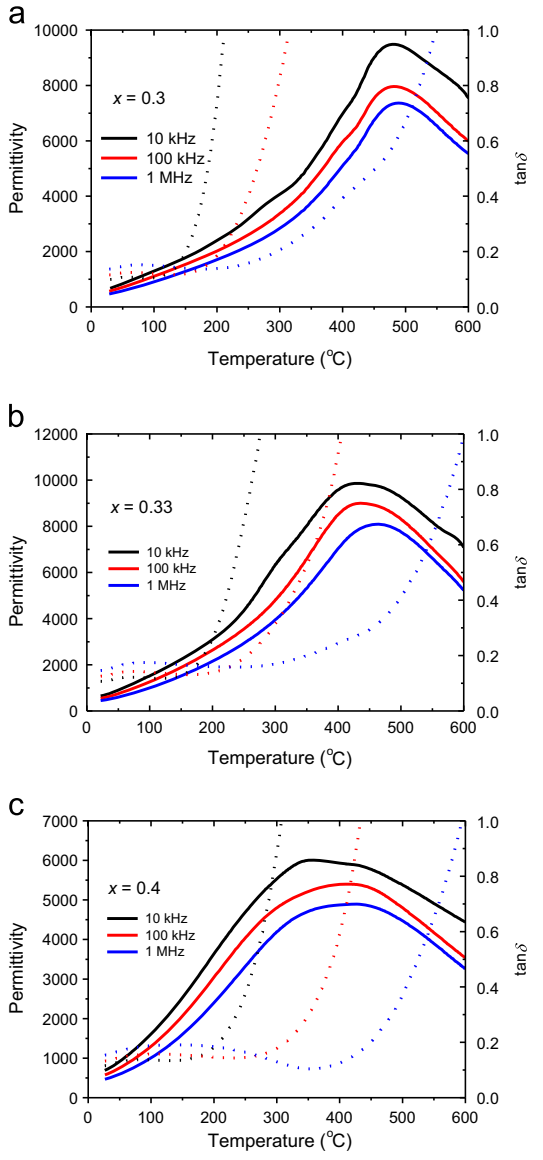

Fig. 5. Frequency dependence of dielectric permittivity (solid lines) and loss (dotted lines) as a function of temperature for the $(1-x)BiFeO_3$–$xBaTiO_3$ solid solutions.

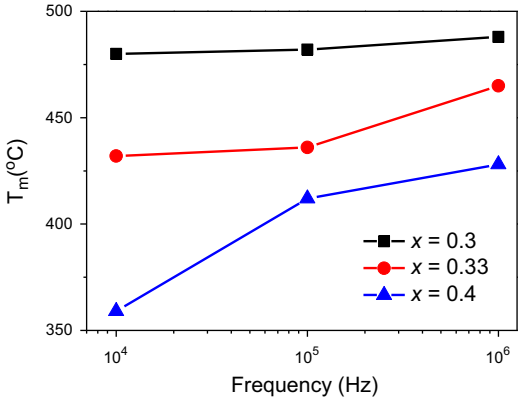

Fig. 6. Variation of maximum permittivity temperature T_m with frequency for the $(1-x)BiFeO_3$–$xBaTiO_3$ solid solutions.

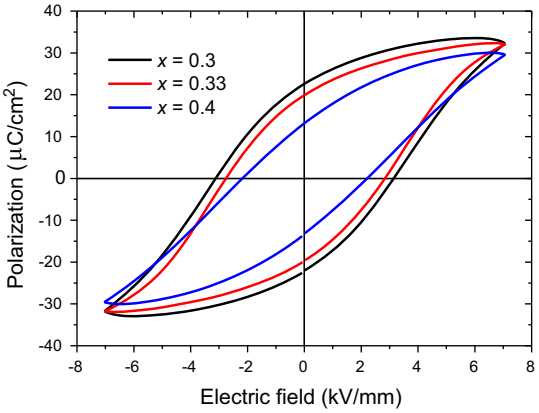

Fig. 7. Ferroelectric hysteresis loops for the $(1-x)BiFeO_3$–$xBaTiO_3$ ceramic samples.

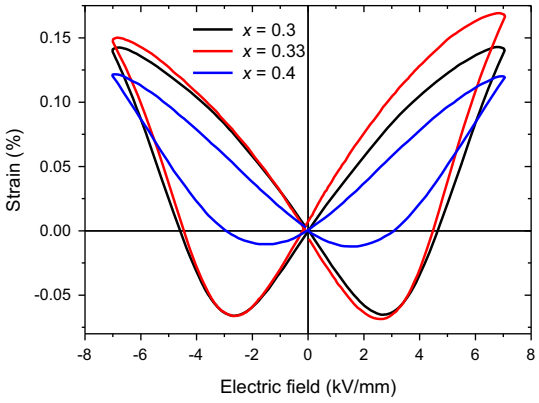

Fig. 8. Bipolar strain curves for the $(1-x)BiFeO_3$–$xBaTiO_3$ ceramic samples.

3.4. Polarization-electric field loops

Fig. 7 shows the *P*–*E* loops for the $BiFeO_3$–$BaTiO_3$ ceramic samples measured at a maximum electric field of 7 kV/mm. Typical ferroelectric hysteresis loops were obtained in the $BiFeO_3$–$BaTiO_3$ solid solutions. Interestingly, the cubic-structured $0.6BiFeO_3$–$0.4BaTiO_3$ still exhibits ferroelectric behavior. In fact, the current cubic-structured $(1-x)BiFeO_3$–$xBaTiO_3$ ($x=0.4$, 0.5) appears to possess some non-cubicity, possibly in the form of polar nanoregions of rhombohedral symmetry [25]. The $BiFeO_3$–$BaTiO_3$ is known to freeze into a random array of polar nanoregions in a spin-glass-like state [13]. Under high electric fields, the polar nanoregions can form macroscale ferroelectric domains, leading to observed ferroelectricity at low temperatures.

As shown in Fig. 7, both the remanent polarization P_r and coercive field E_c were redcued with increasing $BaTiO_3$ content. The P_r and E_c values are listed in Table 1. For comparison, the P_r value of 19.6 μC/cm^2 for $x=0.33$ is higher than 15.2 μC/cm^2 reported for Mn-modified $0.67BiFeO_3$–$0.33BaTiO_3$ [5]. The $0.7BiFeO_3$–$0.3BaTiO_3$ sample exhibited $P_r=22.4$ μC/cm^2 and $E_c=3.2$ kV/mm that are comparable to 15.1 μC/cm^2 and 5.4 kV/mm reported [14].

3.5. Electric field-induced strains

Fig. 8 shows the bipolar strain curves for the $BiFeO_3$–$BaTiO_3$ ceramic samples measured at a maximum electric field of 7 kV/mm. Characteristic "butterfly" strain loops were found. The $x=0.33$ sample exhibited the highest strain among the compositions presented. This composition is characterized as the phase boundary and thus promotes piezoelectric activity [37]. It is notable that the cubic-structured $0.6BiFeO_3$–$0.4BaTiO_3$ sample attained a significant strain of 0.12% at 7 kV/mm. For comparison, the rhombohedral-structured $BiFeO_3$–$BaTiO_3$ ($x=0.3$) displayed larger strains than the cubic-structured $BiFeO_3$–$BaTiO_3$ ($x=0.4$).

4. Conclusions

(1) The XRD characterization shows that pure phase $(1-x)BiFeO_3$–$xBaTiO_3$ solid solutions were produced by the solid-state reaction method. The $x \leq 0.3$ compositions had a rhombohedral symmetry and the $x \geq 0.4$ compositions a cubic symmetry, leaving a rhombohedral-to-cubic phase boundary at $x=0.33$.

(2) The $(1-x)BiFeO_3$–$xBaTiO_3$ solid solutions are revealed to have high maximum temperatures T_m, which were higher than 300 °C in the compositional range of $0.2 \leq x \leq 0.5$.

(3) The electric field-induced strains for cubic-structured $0.6BiFeO_3$–$0.4BaTiO_3$ were found to show a strain of 0.12% at the electric field of 7 kV/mm.

(4) The $BiFeO_3$–$BaTiO_3$ possesses reasonable dielectric properties and electric field-induced strains in combination with high maximum temperatures of use, which enables its use at high temperatures as a lead-free electroceramic.

Acknowledgments

H.L.Z. was supported by the China Scholarship Council (CSC) through Grant no. 2010811389 to cover his stay in Germany for research.

References

[1] F.P. Gheorghiu, A. Ianculescu, P. Postolache, N. Lupu, M. Dobromir, D. Luca, L. Mitoseriu, Preparation and properties of $(1-x)BiFeO_3$–$xBaTiO_3$ multiferroic ceramics, Journal of Alloys and Compounds 506 (2010) 862–867.

[2] M.T. Buscaglia, L. Mitoseriu, V. Buscaglia, I. Pallecchi, M. Viviani, P. Nanni, A.S. Siri, Preparation and characterization of the magneto-electric $xBiFeO_3$–$(1-x)BaTiO_3$ ceramics, Journal of the European Ceramic Society 26 (2006) 3027–3030.

[3] M.M. Kumar, A. Srinivas, S.V. Suryanarayana, Structure property relations in $BiFeO_3$/$BaTiO_3$ solid solutions, Journal of Applied Physics 87 (2000) 855–862.

[4] J. Rödel, W. Jo, K.T.P. Seifert, E.M. Anton, T. Granzow, D. Damjanovic, Perspective on the development of lead-free piezoceramics, Journal of the American Ceramic Society 92 (2009) 1153–1177.

[5] S.O. Leontsev, R.E. Eitel, Dielectric and piezoelectric properties in Mn-modified $(1-x)BiFeO_3$–$xBaTiO_3$ ceramics, Journal of the American Ceramic Society 92 (2009) 2957–2961.

[6] R.C. Turner, P.A. Fuierer, R.E. Newnham, T.R. Shrout, Materials for high temperature acoustic and vibration sensors: a review, Applied Acoustics 41 (1994) 299–324.

[7] Y.P. Wang, G.L. Yuan, X.Y. Chen, J.M. Liu, Z.G. Liu, Electrical and magnetic properties of single-phased and highly resistive ferroelectro-magnet $BiFeO_3$ ceramic, Journal of Physics D: Applied Physics 39 (2006) 2019–2023.

[8] H. Singh, A. Kumar, K.L. Yadav, Structural, dielectric, magnetic, magnetodielectric and impedance spectroscopic studies of multiferroic $BiFeO_3$–$BaTiO_3$ ceramics, Materials Science and Engineering B 176 (2011) 540–547.

[9] J.S. Kim, C.I. Cheon, P.W. Jang, Y.N. Choi, C.H. Lee, Ferroelectric and ferromagnetic properties of $0.2BiFeO_3$–$0.2RFeO_3$–$0.6ATiO_3$ (R=Pr, Nd and A=Ba, Pb) and $0.8BiFeO_3$–$0.2BaTiO_3$, Journal of the European Ceramic Society 24 (2004) 1551–1555.

[10] M.M. Kumar, S. Srinath, G.S. Kumar, S.V. Suryanarayana, Spontaneous magnetic moment in $BiFeO_3$-$BaTiO_3$ solid solutions at low temperatures, Journal of Magnetism and Magnetic Materials 188 (1998) 203–212.

[11] T.H. Wang, Y. Ding, C.S. Tu, Y.D. Yao, K.T. Wu, T.C. Lin, H.H. Yu, C.S. Ku, H.Y. Lee, Structure, magnetic, and dielectric properties of $(1-x)BiFeO_3$-$xBaTiO_3$ ceramics, Journal of Applied Physics 109 (2011) 07D907.

[12] C.Y. Shi, X.Z. Liu, Y.M. Hao, Z.B. Hu, Structural, magnetic and dielectric properties of Sc modified $(1-y)BiFeO_3$–$yBaTiO_3$ ceramics, Solid State Science 13 (2011) 1885–1888.

[13] G.A. Samara, The relaxational properties of compositionally disordered ABO_3 perovskites, Journal of Physics: Condensed Matter 15 (2003) R367–R411.

[14] K.C. Verma, R.K. Kotnala, Multiferroic magnetoelectric coupling and relaxor ferroelectric behavior in $0.7BiFeO_3$–$0.3BaTiO_3$ nanocrystals, Solid State Communications 151 (2011) 920–923.

[15] J.M. Moreau, C. Michel, R. Gerson, W.J. James, Ferroelectric $BiFeO_3$ X-ray and neutron diffraction study, Journal of Physics and Chemistry of Solids 32 (1971) 1315–1320.

[16] T.H. Wang, C.S. Tu, Y. Ding, T.C. Lin, C.S. Ku, W.C. Yang, H.H. Yu, K.T. Wu, Y.D. Yao, H.Y. Lee, Phase transition and ferroelectric properties of $xBiFeO_3$–$(1-x)BaTiO_3$ ceramics, Current Applied Physics 11 (2011) S240–S243.

[17] J.F. Scott, Ferroelectrics go bananas, Journal of Physics: Condensed Matter 20 (2008) 021001.

[18] J.R. Cheng, L.E. Cross, Effects of La substituent on ferroelectric rhombohedral/tetragonal morphotropic phase boundary in $(1-x)$(Bi,La)$(Ga_{0.05}Fe_{0.95})O_3$–$xPbTiO_3$ piezoelectric ceramics, Journal of Applied Physics 94 (2003) 5188–5192.

[19] T.P. Comyn, T.J. Stevenson, A.J. Bell, Piezoelectric properties of $BiFeO_3$-$PbTiO_3$ ceramics, Journal of Physics IV 128 (2005) 13–17.

[20] X.H. Liu, Z. Xu, X.Y. Wei, X. Yao, Ferroelectric and ferromagnetic properties of $0.7BiFe_{1-x}Cr_xO_3$–$0.3BaTiO_3$ solid solutions, Journal of the American Ceramic Society 91 (2008) 3731–3734.

[21] J.S. Kim, C.I. Cheon, H.J. Kang, P.W. Jang, High temperature properties of multiferroic $BiFeO_3$–$DyFeO_3$–$BaTiO_3$ solid solutions, Journal of the European Ceramic Society 27 (2007) 3951–3954.

[22] J. Wang, J.B. Neaton, H. Zheng, V. Nagarajan, S.B. Ogale, B. Liu, D. Viehland, V. Vaithyanathan, D.G. Schlom, U.V. Waghmare, N.A. Spaldin, K.M. Rabe, M. Wuttig, R. Ramesh, Epitaxial $BiFeO_3$ multiferroic thin film heterostructures, Science 299 (2003) 1719–1722.

[23] S.O. Leontsev, R.E. Eitel, Origin and Magnitude of the large piezoelectric response in the lead-free $(1-x)BiFeO_3$–$xBaTiO_3$ solid solution, Journal of Materials Research 26 (2011) 9–17.

[24] Y. Yoneda, K. Yoshii, S. Kohara, S. Kitagawa, S. Mori, Local structure of $BiFeO_3$-$BaTiO_3$ mixture, Japanese Journal of Applied Physics 47 (2008) 7590–7594.

[25] T. Ozaki, S. Mori, Dielectric properties and related domain structures in $0.75BiFeO_3$–$0.25BaTiO_3$, Japanese Journal of Applied Physics 48 (2009) 09KC07.

[26] H. Bea, B. Ziegler, M. Bibes, A. Barthelemy, P. Paruch, Nanoscale polarization switching mechanisms in multiferroic $BiFeO_3$ thin films, Journal of Physics: Condensed Matter 23 (2011) 142201.

[27] J.B. Goodenough, J.M. Longo, Landolt-Bornstein Group III, Magnetic and Other Properties of Oxides and Related Compounds, vol. 4, Springer-Verlag, New York, 1970.

[28] M.M. Kumar, A. Srinivas, S.V. Suryanarayana, T. Bhimasankaram, Dielectric and impedance studies on $BiFeO_3$-$BaTiO_3$ solid solutions, Physica Status Solidi A 165 (1998) 317–326.

[29] S.W. Zhang, H.L. Zhang, B.P. Zhang, S. Yang, Phase-transition behavior and piezoelectric properties of lead-free $(Ba_{0.95}Ca_{0.05})(Ti_{1-x}Zr_x)O_3$ ceramics, Journal of Alloys and Compounds 506 (2010) 131–135.

[30] B.P. Zhang, J.F. Li, K. Wang, H.L. Zhang, Compositional dependence of piezoelectric properties in $Na_xK_{1-x}NbO_3$ lead-free ceramics prepared by spark plasma sintering, Journal of the American Ceramic Society 89 (2006) 1605–1609.

[31] R. Guo, L.E. Cross, S.E. Park, B. Noheda, D.E. Cox, G. Shirane, Origin of the high piezoelectric response in $PbZr_{1-x}Ti_xO_3$, Physical Review Letters 84 (2000) 5423–5426.

[32] B. Fraygola, J.A. Eiras, Intrinsic magnetoelectric coupling in PFW-PT solid solutions, Solid State Communications 158 (2013) 54–57.

[33] P. Uniyal, K.L. Yadav, Room temperature multiferroic properties of Eu doped $BiFeO_3$, Journal of Applied Physics 105 (2009) 07D914.

[34] Y.X. Wei, X.T. Wang, J.J. Jia, X.L. Wang, Multiferroic and piezoelectric properties of $0.65BiFeO_3$–$0.35BaTiO_3$ ceramic with pseudo-cubic symmetry, Ceramics International 38 (2012) 3499–3502.

[35] E.M. Anton, W. Jo, D. Damjanovic, J. Rödel, Determination of depolarization temperature of $(Bi_{1/2}Na_{1/2})TiO_3$-based lead-free piezoceramics, Journal of Applied Physics 110 (2011) 094108.

[36] S.W. Zhang, H.L. Zhang, B.P. Zhang, G.L. Zhao, Dielectric and piezoelectric properties of $(Ba_{0.95}Ca_{0.05})(Ti_{0.88}Zr_{0.12})O_3$ ceramics sintered in a protective atmosphere, Journal of the European Ceramic Society 29 (2009) 3235–3242.

[37] D. Damjanovic, A morphotropic phase boundary system based on polarization rotation and polarization extension, Applied Physics Letters 97 (2010) 062906.